Designing power heterojunction bipolar transistors with non-uniform emitter finger lengths to achieve high thermal stability*

Jin Dong-Yue(金冬月)†, Zhang Wan-Rong(张万荣), Fu Qiang(付 强), Chen Liang(陈 亮), Xiao Ying(肖 盈), Wang Ren-Qing(王任卿), and Zhao Xin(赵 昕)

College of Electronic Information and Control Engineering, Beijing University of Technology, Beijing 100124*, China*

(Received 15 December 2010; revised manuscript received 16 February 2011)

With the aid of a thermal-electrical model, a practical method for designing multi-finger power heterojunction bipolar transistors with finger lengths divided in groups is proposed. The method can effectively enhance the thermal stability of the devices without sacrificing the design time. Taking a 40-finger heterojunction bipolar transistor for example, the device with non-uniform emitter finger lengths is optimized and fabricated. Both the theoretical and the experimental results show that, for the optimum device, the peak temperature is lowered by 26.19 K and the maximum temperature difference is reduced by 56.67% when compared with the conventional heterojunction bipolar transistor with uniform emitter finger length. Furthermore, the ability to improve the uniformity of the temperature profile and to expand the thermal stable operation range is strengthened as the power level increases, which is ascribed to the improvement of the thermal resistance in the optimum device. A detailed design procedure is also summarized to provide a general guide for designing power heterojunction bipolar transistors with non-uniform finger lengths.

Keywords: heterojunction bipolar transistor, high power, thermal stability

PACS: 44.10.+i, 73.40.Lq, 91.60.Ki **DOI:** 10.1088/1674-1056/20/7/074401

1. Introduction

In many high-power circuit applications, heterojunction bipolar transistors (HBTs) employ the multiple fingers structure with uniform emitter finger length to spread the current and to dissipate the heat. However, the self-heating effect caused by the power dissipation and the thermal-coupling effect among emitter fingers result in an uneven temperature profile and give rise to the thermal instability of the power HBTs, which confines their power handling capability to a level considerably lower than the electronic limitation. Therefore, enhancing thermal stability has become a critical issue for the power HBTs.[1−4]

In order to improve the non-uniformity of the temperature profile and to enhance the thermal stability, the structure with non-uniform emitter finger lengths has been used.[5,6] By decreasing the lengths of the center emitter fingers, the heat caused by the power consumption in the central region is reduced markedly. At the same time, as the thermal coupling effect only comes from one direction for the outmost fingers, these side emitter fingers are more efficient for spreading heat, therefore, the lengths of these side emitter fingers could be increased moderately to keep the total emitter finger length unchanged. For the HBT with several fingers, such as 10 fingers, the design of non-uniform emitter fingers is straightforward. However, for the device with dozens of fingers, assigning a different length for each finger will become non-trivial and time-consuming.

In this paper, based on a thermal-electrical model, a relative convenient and quick method to design the emitter finger lengths in groups is presented. The design can effectively enhance the thermal characteristics of the multi-finger power HBTs. Taking a 40-finger HBT for example, a detailed procedure to design an HBT with non-uniform emitter finger lengths

*Project supported by the National Natural Science Foundation of China (Grant Nos. 61006059, 60776051, and 61006044), the Beijing Municipal Natural Science Foundation of China (Grant No. 4082007), the National Basic Research Program of China, the Beijing Municipal Education Committee of China (Grant Nos. KM200710005015 and KM200910005001), the Beijing Municipal Trans-century Talent Project of China (Grant No. 67002013200301), the Beijing Innovatory Talent Training Program of China (Grant No. 00200054RA001), and the Ph. D. Start Science Foundation of Beijing University of Technology, China (Grant No. X0002013201102).

†Corresponding author. E-mail: dyjin@bjut.edu.cn

© 2011 Chinese Physical Society and IOP Publishing Ltd

is presented. Furthermore, the optimum 40-finger HBT was fabricated and the temperature profile and the common–emitter current (I_C)–voltage (V_{BE}) characteristics were measured. Both the simulation and the measurement show that the optimum device could improve the thermal stability effectively, thus confirm the feasibility of the practical design method.

2. Thermal-electrical model

Before designing the structure with non-uniform finger lengths, a thermal-electrical model[7−9] is applied to calculate the temperature profile of the multi-finger HBT. Figure 1 shows the three-dimensional schematic diagram of a power HBT with K emitter fingers, where L, W and d are the chip sizes in the directions of x, y and z, respectively. Considering the non-uniformity of the temperature in a given emitter finger, each one is divided into $M_k \times N_k$ heat-source cells, each with coordinates of $x_{k,ij}$ and $y_{k,ij}$ in the k-th emitter finger ($k = 1, 2, \ldots, K$) and with geometry of l and w. The current and the temperature are assumed to be uniform on the surface of each individual heat-source cell.

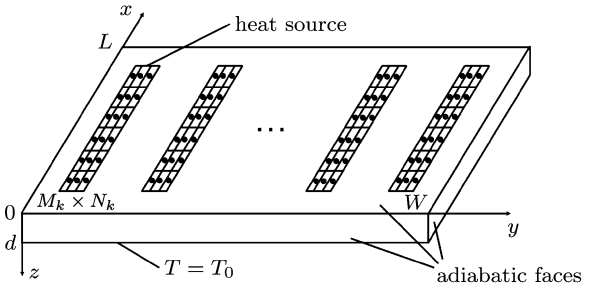


Fig. 1. The three-dimensional schematic diagram of a multi-finger power HBT.

In a steady state, the temperature profile of the device can be determined with the heat flow equation

$$\nabla^2 T(x, y, z) = 0, \tag{1}$$

and the appropriate boundary conditions

$$T|_{z=d} = T_0, \tag{2}$$

$$K_{\text{th}} \left.\frac{\partial T}{\partial z}\right|_{z=0} = -p(x, y), \tag{3}$$

$$\left.\frac{\partial T}{\partial x}\right|_{x=0,L} = 0, \tag{4}$$

$$\left.\frac{\partial T}{\partial y}\right|_{y=0,W} = 0, \tag{5}$$

where the bottom of the chip ($z = d$) is fixed at the ambient temperature T_0 (300 K in our study), the heat source is assumed to be located on the top surface ($z = 0$), $p(x, y)$ is a distribution function of the input power density on the chip's top surface, which is zero except at the fingers where the device power is dissipated and K_{th} is the thermal conductivity of the substrate materials.

With a separation of variables, the analytical solution for the heat flow Eq. (1) can be obtained with the appropriate boundary conditions given by Eqs. (2)–(5). Most often we are interested in the temperature profiles on the top surface. Therefore, only the expression for the top surface temperature $T(x, y, 0)$ is given:

$$\begin{aligned}
&T(x, y, 0) \\
&= \frac{2w}{LW} \sum_{m=1}^{\infty} \left[\frac{1}{\lambda_m^2} \tanh(\lambda_m d) \sum_{k=1}^{K} \sum_{i=1}^{M_k} \sum_{j=1}^{N_k} \frac{p_{k,ij}}{K_{\text{th}}} \right. \\
&\left. \times F(m, k, i, j) \cdot \cos(\lambda_m x) \right] \\
&+ \frac{2l}{LW} \sum_{n=1}^{\infty} \left[\frac{1}{\mu_n^2} \tanh(\mu_n d) \sum_{k=1}^{K} \sum_{i=1}^{M_k} \sum_{j=1}^{N_k} \frac{p_{k,ij}}{K_{\text{th}}} \right. \\
&\left. \times G(n, k, i, j) \cdot \cos(\mu_n y) \right] \\
&+ \frac{4}{LW} \sum_{m=1}^{\infty} \sum_{n=1}^{\infty} \left\{ \frac{1}{\lambda_m \mu_n \gamma} \tanh(\gamma d) \right. \\
&\times \sum_{k=1}^{K} \sum_{i=1}^{M_k} \sum_{j=1}^{N_k} \left[\frac{p_{k,ij}}{K_{\text{th}}} \cdot F(m, k, i, j) \right. \\
&\left. \left. \times G(n, k, i, j) \cdot \cos(\lambda_m x) \cdot \cos(\mu_n y) \right] \right\} \\
&+ \frac{lwd}{LW} \sum_{k=1}^{K} \sum_{i=1}^{M_k} \sum_{j=1}^{N_k} \frac{p_{k,ij}}{K_{\text{th}}} + T_0,
\end{aligned} \tag{6}$$

where

$$\lambda_m = m\pi/L, \quad \mu_n = n\pi/W, \quad \gamma^2 = \lambda_m^2 + \mu_n^2,$$
$$F(m, k, i, j) = \sin \lambda_m (x_{k,ij} + l/2) - \sin \lambda_m (x_{k,ij} - l/2),$$
$$G(n, k, i, j) = \sin \mu_n (y_{k,ij} + w/2) - \sin \mu_n (y_{k,ij} - w/2).$$

Taking into account the positive temperature coefficient of I_C, which means that there is a negative temperature coefficient for the base-emitter voltage (ϕ), the expressions for the collector current density ($J_{ck,ij}$) and for the power density ($p_{k,ij}$) of the (i, j) heat-source cell in the k-th finger of the power HBT are given by

$$\begin{aligned}
J_{ck,ij} &= J_{c0} \exp \left\{ \frac{q}{k_0 T_0} [V_{\text{BE}} - \phi T(x_{k,ij}, y_{k,ij}, 0) \right. \\
&\left. + \phi T_0] \right\},
\end{aligned} \tag{7}$$

$$p_{k,ij} = J_{ck,ij} \cdot V_{\text{CE}}, \tag{8}$$

where J_{c0} is the saturation current, k_0 is the Boltzmann constant, q is the charge of an electron, V_{BE} and V_{CE} are the voltages of base–emitter and collector–emitter, respectively.

Considering the effect of thermal-electrical feedback, the Gummel approach, namely the self-consistent iteration approach, is applied to solve Eqs. (6)–(8). We first assume that the collector currents in all the heat-cells are the same. A preliminary temperature profile is evaluated with Eq. (6), and the temperature profile is used to recalculate a current distribution with Eq. (7). Afterwards, the updated current distribution is used to recalculate the temperature profile. The process is repeated until a self-consistent solution exists simultaneously for both the temperature profile and the current distribution.

3. Structure design

With the aid of the thermal-electrical model, the top surface temperature profile in the active region of a 10-finger HBT with total emitter stripe area of 40 μm×10 μm and a uniform length of 40 μm is calculated, which shows a higher temperature at the center fingers (Fig. 2(a)). For the 10-finger HBT, the emitter finger length values are assumed to be L_1, L_2, ..., L_{10}, where L_5 and L_6 denote the center lengths. Considering the symmetry, there are only 5 length values to be assigned. If we designed a structure with non-uniform length values ($L_1 = L_{10} = 50$ μm, $L_2 = L_9 = 45$ μm, $L_3 = L_8 = 40$ μm, $L_4 = L_7 = 35$ μm and $L_5 = L_6 = 30$ μm) and with vertical structure, total emitter stripe area and total length identical to those of the uniform one, the temperature profile is markedly improved as shown in Fig. 2(b). The HBT with non-uniform emitter finger lengths has a lower peak temperature of 343.8 K, which is lowered by 24.83 K when compared with that of the uniform one. Furthermore, the maximum temperature difference of the top surface is reduced by 53.51% and the fingers are operating nearly at the same temperature, which effectively suppresses the positive current–temperature feedback and hence improve the thermal stability of the power device.

To design the fingers with non-uniform lengths for an HBT with more than 10 fingers, assigning a different value to each finger length such as the aforementioned approach becomes non-trivial and very time-consuming. A relative easy and quick method to design the emitter lengths in several groups is proposed to improve the uniformity of the temperature profile.

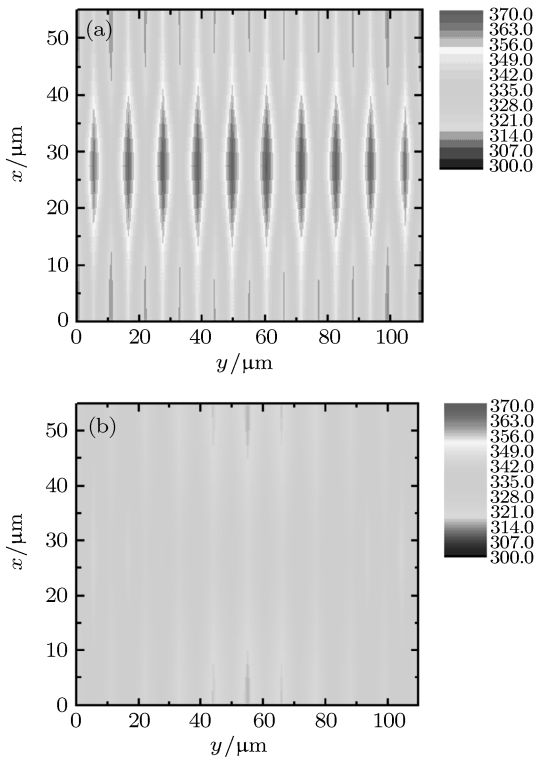


Fig. 2. Temperature profiles for a 10-finger HBT (a) with uniform emitter finger length and (b) with non-uniform emitter finger lengths. The active region size (55 μm×110 μm), total emitter stripes area (400 μm^2), total finger length (400 μm) and the dissipated power (0.5 W at $V_{CE} = 5$ V and $I_C = 0.1$ A) are identical in both figures.

Taking a 40-finger HBT for example, a detailed procedure to design the emitter lengths in groups is presented, wherein the device has an active region size of 55×440 μm^2, a total emitter stripe area of 40×40 μm^2, and the same vertical structure as the aforementioned 10-finger HBT. We start from a uniform length of 40 μm for each finger, as shown in Table 1(device A). First, considering the symmetry, there are 20 length values to be designed. The length values are assumed to be L_1, L_2, ..., L_{20}, where L_{20} denotes the center finger length. Second, the 20 lengths are divided into 5 groups. There are 4 lengths, which are equal to each other, in each group. Clearly, there are only 5 emitter lengths to be designed and the time required to design the 40-finger HBT is close to that for a 10-finger HBT. Considering that the structures for the 40-finger and the 10-finger HBTs are similar, the above mentioned optimum length values (50–45–40–35–30–30–35–40–45–50 μm) for the 10-finger HBT could be adopted to the 40-finger HBT. Letting the values in each groups corresponding to the optimum length values for the 10-finger HBT, we could present the detail length values in Table 1(device B).

Table 1. Emitter finger length values for two types of 40-finger power HBTs.

Power HBTs	Emitter finger length values of 40-finger HBTs/μm									
	L_1–L_4	L_5–L_8	L_9–L_{12}	L_{13}–L_{16}	L_{177}–L_{20}	L_{21}–L_{24}	L_{25}–L_{28}	L_{29}–L_{32}	L_{33}–L_{36}	L_{37}–L_{40}
Device A	40	40	40	40	40	40	40	40	40	40
Device B	50	45	40	35	30	30	35	40	45	50

The temperature profiles of 40-finger HBTs with uniform finger length (device A) and non-uniform finger lengths (device B) are shown in Figs. 3(a) and 3(b), respectively. Clearly, for device B, the peak temperature is lowered by 26.19 K and the maximum temperature difference is only 31.87 K, which is reduced by 56.67% when compared with that of device A.

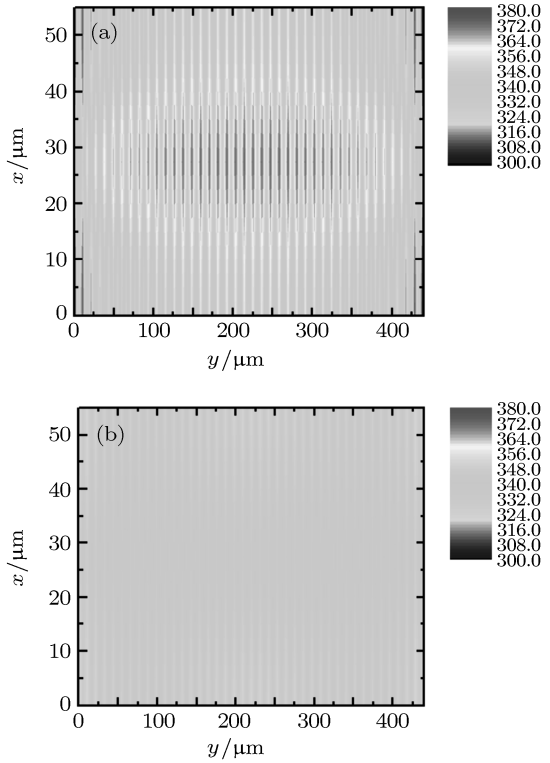


Fig. 3. Temperature profiles for the 40-finger HBTs: (a) device A, (b) device B. The active region size (55 μm×440 μm), the total emitter stripe area (1600 μm^2), the total emitter finger length (1600 μm) and the dissipated power (2 W at V_{CE} = 5 V and I_C = 0.4 A) are identical in both figures.

4. Device fabrication

To illustrate the efficiency of the design method in experiment, both devices A and B were fabricated by the double mesa SiGe HBT process. Figure 4 shows the vertical structure of the fabricated SiGe HBTs. The collector region with a nominal thickness of 3.48 μm and a lightly doping concentration of 1×10^{16} cm^{-3} is designed to realize a high breakdown voltage. A normal Ge doping (16%) is used to maintain a valence band offset between the emitter and the base, which permits a high doping concentration (2×10^{19} cm^{-3}) to be employed in a thin (30 nm) base region and still maintains reasonable current gain values. In order to reduce the boron out-diffusion during the chemical vapor deposition (CVD) and the processing, intrinsic SiGe spacers (5 nm and 15 nm)

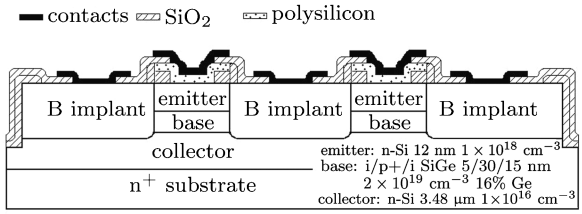


Fig. 4. The vertical structure of a SiGe HBT with multiple emitter fingers.

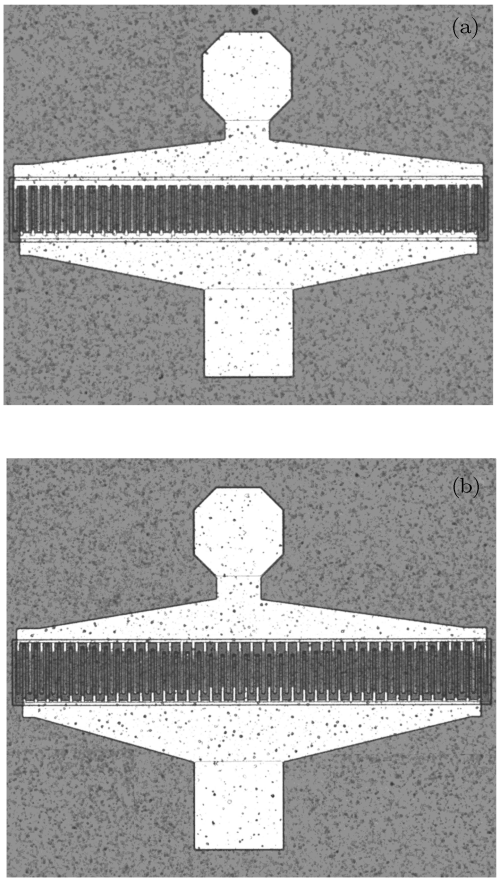


Fig. 5. Micrographs of the surface view of fabricated 40-finger power SiGe HBTs: (a) device A, (b) device B.

are made adjacent to the base region during the epi-growth of the SiGe base, respectively. The emitter region is designed with a nominal thickness of 12 nm and a normal doping concentration of 1×10^{18} cm^{-3}. The double-mesa SiGe HBT process used in this paper will not be described here; the reader is referred to the previous publication[10] for details. The micrographs of the surface view of the fabricated devices A and B are shown in Figs. 5(a) and 5(b), respectively.

5. Results and discussion

To check the improvement of the temperature profile in device B, both temperature profiles of devices A and B were measured with an infrared micro imager. At the same time, considering that the maximum temperature of each finger is located at the central region, both the experimental and the theoretical results of the temperature profiles along the central line across the multi-emitter fingers are presented in Fig. 6 for comparison. The agreement of experiment and theory is excellent, since variations of less than 5 K are found over the central lines of the active regions for both devices. Moreover, the optimum length configuration for device B yields an average temperature of 343.78 K across the multi-emitter fingers, with a standard deviation of 7 K. The average temperature presents a 28.71-K decrease compared to the peak temperature of device A.

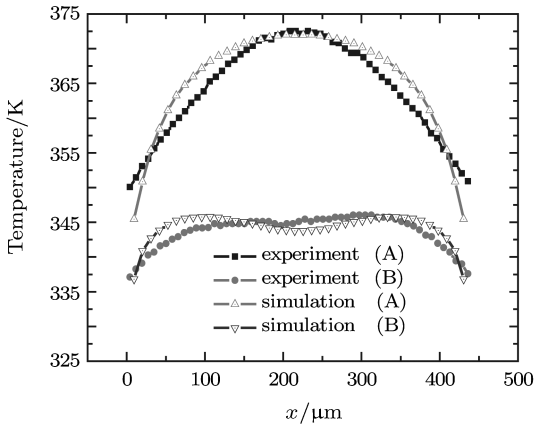


Fig. 6. Experimental and theoretical results of temperature profiles along the central lines across the multi-emitter fingers in devices A and B at the dissipated power of 2 W ($V_{\rm CE} = 5$ V and $I_{\rm C} = 0.4$ A).

Furthermore, the measured temperature profiles of the two devices along the central lines across the multi-emitter fingers at different $I_{\rm C}$'s are shown in Fig. 7. Compared with device A, the improvement of the peak temperature of device B is increased from 6.94 K to 42.54 K, while the non-uniformity of the temperature profile is increased from 38.41% to 55.27%, as $I_{\rm C}$ increases from 0.2 A to 0.6 A. In other words, device B with optimum length configuration can effectively improve the temperature profile over a wide range of collector currents (namely the power levels).

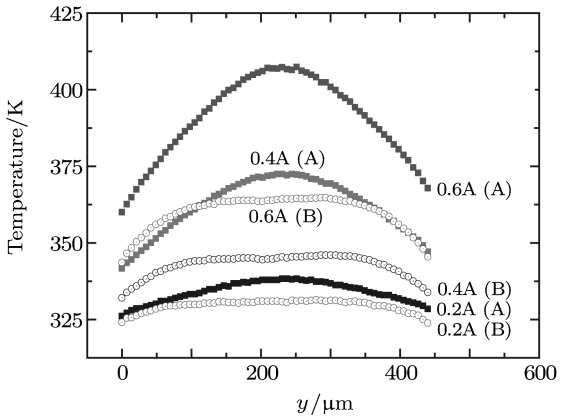


Fig. 7. Temperature profiles along central lines in devices A and B under different $I_{\rm C}$'s at $V_{\rm CE} = 5$ V.

To check the thermal properties of the two devices, the $I_{\rm C}$–$V_{\rm BE}$ curves at different $V_{\rm CE}$'s were also measured by an Agilent 4155C. Figure 8 illustrates the influence of $V_{\rm CE}$ on the $I_{\rm C}$–$V_{\rm BE}$ characteristics in devices A and B. Note that the $I_{\rm C}$–$V_{\rm BE}$ curves bend to left as $V_{\rm CE}$ increases. The $I_{\rm C}$–$V_{\rm BE}$ curve of device B is located at the right-hand side of device A over the entire biasing range. Therefore, the thermal stability of device B is superior to that of device A over the entire biasing range. The improvement of the thermal stability becomes more obviously as $V_{\rm CE}$ increases. Furthermore, it is also illustrated that $V_{\rm BE}$ reaches a maximum value and regresses toward lower values as $I_{\rm C}$ increases at $V_{\rm CE} = 9$ V. In other words, both devices are in thermal instability state. However, the power level for thermal instability of device B is still higher than that of device A.

The power levels of thermal instability ($P_{\rm DC}$) in two devices are measured at different $V_{\rm CE}$'s and are shown in Fig. 9. The $P_{\rm DC}$'s of both devices decrease as $V_{\rm CE}$ increases from 7 V to 10 V. However, the $P_{\rm DC}$ of device B is higher than that of Device A over the entire biasing range. To conveniently show the improvement of the $P_{\rm DC}$ in device B, the factor ζ of $P_{\rm DC}$ is defined as $\zeta = (P_{\rm DCB} - P_{\rm DCA})/P_{\rm DCA}$, where $P_{\rm DCA}$ and $P_{\rm DCB}$ are the power levels of thermal instability of devices A and B, respectively. It is shown clearly that ζ increases as $V_{\rm CE}$ increases from 7 V to 10 V,

which means that for device B, the ability to enhance the power level of thermal instability is strengthened.

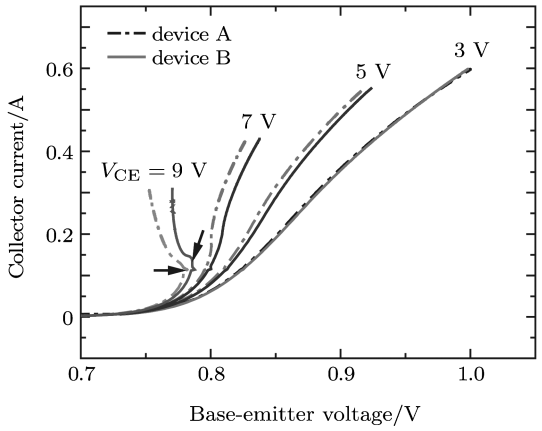


Fig. 8. Dependence of I_C–V_{BE} characteristics on collector-current voltage V_{CE} (at 3 V, 5 V, 7 V and 9 V). Arrows indicate the regression points.

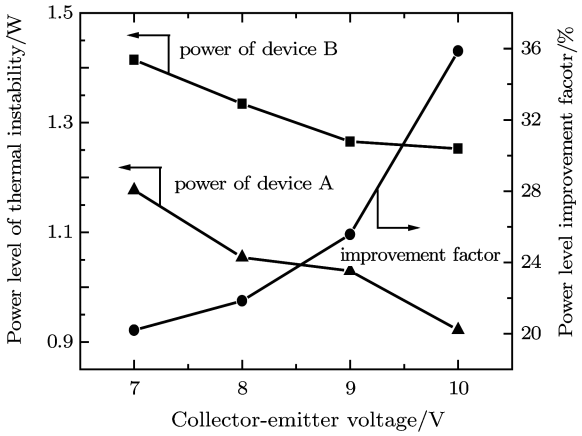


Fig. 9. The comparison of the power levels of thermal instability in devices A and B. Dependence of I_C–V_{BE} characteristics on collector-current voltage V_{CE} (at 7 V, 8 V, 9 V and 10 V).

The thermal resistance is also presented to compare the thermal properties of the devices. The thermal resistance R_{th} defined by the following equation shows the ratio of the increase of the junction temperature to the power consumption:[11]

$$R_{th} = \frac{(1/\phi)\Delta V_{BE}}{I_C \Delta V_{CE}}, \tag{9}$$

where ΔV_{BE} and ΔV_{CE} represent changes in V_{BE} and V_{CE} with the power change while keeping I_C at a constant, the value of ϕ can be experimentally determined. In our fabricated SiGe HBTs, the typical value of ϕ is -1.71 mV/°C, which is consistent with the value given in Ref. [12].

In Fig. 10, the thermal resistance improvement factor γ of device B versus V_{CE} at $I_C = 0.4$ A is presented, where γ is defined as $\gamma = (R_{thA} - R_{thB})/R_{thA}$ and R_{thA} and R_{thB} are the thermal resistances of devices A and B, respectively. It is shown that the R_{th} of device B is always less than that of device A, and device B reveals a 10.44% to 28.44% reduction of R_{th} as V_{CE} increases. The decrease of R_{th} in device B results in an increase in the regression points and hence produces an expansion of the thermal stable operation range.

Both the theoretical and the experimental results show that the uniformity of the temperature profile and the thermal stability of the power HBT are effectively improved by designing the non-uniform finger lengths in groups, which does not sacrifice the design time. The detailed design procedure can be summarized as follows.

1) Confirm the number of emitter length values to be assigned. For an N-finger HBT, considering the symmetry, the number of emitter length values is decreases to $N/2$ if N is an even integer, or $(N+1)/2$ if N is an odd integer.

2) Divide the emitter lengths into several groups. The length values in each group are equal to each other. As a result, the number of emitter length values is further decreased.

3) With the aid of the thermal-electrical model, decrease the lengths of the center groups and increase the lengths of the outside groups moderately while keep the total finger length value unchanged. As a result, the non-uniformity of the temperature profile and the thermal stability of power HBT are effectively improved and the design work is finalized.

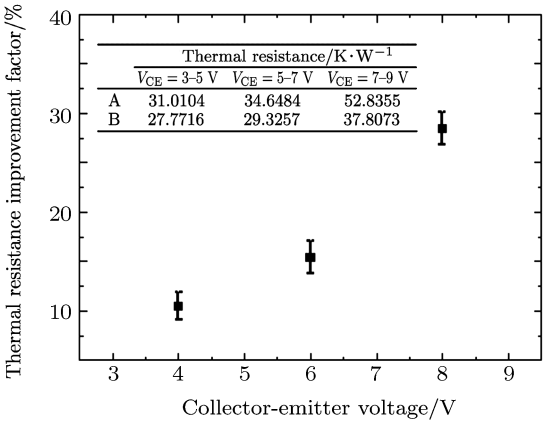


Fig. 10. The thermal resistance improvement factor of device B versus V_{CE} at $I_C = 0.4$ A. The thermal resistance of two devices at different V_{CE}'s is also shown in the insert table.

6. Conclusion

As the conventional method to assign a different value to each finger length in multi-finger power HBT

is non-trivial and time-consuming, a practical method to design power HBTs with non-uniform emitter finger lengths in groups has been proposed. The design can effectively improve the uniformity of the temperature profile and enhance the thermal stability. Taking a 40-finger HBT for example, a detailed design procedure is presented without the non-trivial and time-consuming design process. With the aid of a thermal-electrical model, the temperature profile of the HBT with optimum finger lengths (device B) is calculated, which shows that the peak temperature is lowed by 26.19 K and the maximum temperature difference is reduced by 56.67% when compared with that of the uniform length one (device A). Furthermore, the optimum 40-finger HBT is fabricated by the double mesa SiGe HBT process. The agreement between the calculated temperature profile and the measured one is excellent. The common–emitter $I_{\rm C}$–$V_{\rm BE}$ characteristics are also measured. And the power level of thermal instability and the thermal resistance are also compared for the two devices. Compared with device A, device B with optimum non-uniform finger lengths always has smaller $R_{\rm th}$ and reveals a 10.44% to 28.44% reduction of $R_{\rm th}$ as$V_{\rm CE}$ increases. The decrease of $R_{\rm th}$ results in an increase in the regression points and hence produces an expansion of the thermal stable operation range which confirms the efficiency of the design method. The results of this work provide useful guidelines for designing power HBTs with good thermal stability over a wide biasing range.

References

[1] Avenier G, Diop M, Chevalier P, Troillard G, Loubet N, Bouvier J, Depoyan L, Derrier N, Buczko M, Leyris C, Boret S, Montusclat S, Margain A, Pruvost S, Nicolson S T, Yau K H K, Revil N, Gloria D, Dutartre D, Voinigescu S P and Chantre A 2009 *IEEE J. Solid-State Circuits* **44** 2312

[2] Kou J L, Lu H J, Wu F M and Xu Y S 2009 *Chin. Phys.* B **18** 1553

[3] Ding Y G, Han Y, Liu P K and Liu Y W 2009 *Acta Phys. Sin.* **58** 1806 (in Chinese)

[4] Kim H S, Kim K Y, Kim W Y, Noh Y S, Yom I B, Oh I Y and Park C S 2009 *Electron. Lett.* **45** 1036

[5] Lee J G, Oh T K, Kim B and Kang B K 2001 *Solid-State Electron.* **45** 27

[6] Macchiaroli M, d'Alessandro V and Rinaldi N 2002 *Proceedings of the International Conference on Microelectronics* Nis, Yugoslavia, May 12–15, 2002 p. 455

[7] Gao G B, Wang M Z, Gui X and Morkoc H 1989 *IEEE Trans. Electron. Dev.* **36** 854

[8] Cao B Y and Guo Z Y 2008 *Acta Phys. Sin.* **57** 4273 (in Chinese)

[9] Jin D Y, Zhang W R, Xie H Y, Chen L, Shen P and Hu N 2009 *Microelectronics Reliability* **49** 382

[10] Jin D Y, Zhang W R, Shen P, Xie H Y, Wang Y and Zhang W 2008 *Solid-State Electron.* **52** 937

[11] Liu W, Nelson S, Hill D G and Khatibzadeh A 1993 *IEEE Trans. Electron. Dev.* **40** 1917

[12] McAlister S P, Kovacic S, Renaud A and Zhou Z F 2000 *J. Vac. Sci. Technol.* A **18** 770